High Temperature Intergranular Oxidation of Nickel Based Superalloy Inconel 718

Sudhanva Madhusudan, Enrica Epifano, Jérôme Favergeon, Tom Sanviemvongsak, David Maréchal, Daniel Monceau

High Temperature Corrosion of Materials
https://doi.org/10.1007/s11085-024-10260-z

ORIGINAL PAPER

High Temperature Intergranular Oxidation of Nickel Based Superalloy Inconel 718

Sudhanva Madhusudan[1,3] · Enrica Epifano[1] · Jérôme Favergeon[2] · Tom Sanviemvongsak[4] · David Maréchal[3] · Daniel Monceau[1]

Received: 12 July 2024 / Revised: 12 July 2024 / Accepted: 17 July 2024

Abstract

Intergranular oxidation (IGO) of the Ni-based superalloy Inconel 718 was studied at 650 °C, 700 °C and 900 °C. The oxidized samples were characterized by *X*-ray diffraction and scanning electron microscopy. For all the studied temperatures, the external scale was mainly composed of Cr_2O_3, while the oxides along the grain boundaries were rich in Al and, to a minor extent, Ti. This was consistent with thermodynamic computations. The time evolution of the maximum depth of IGO was found to be parabolic with an apparent activation energy of 164 kJ/mol. The results of this study confirm with three temperatures that IGO kinetics can be described using an extension of the Wagner's theory of internal oxidation, as recently suggested in the literature at 850 °C. According to this description, the mechanisms controlling the IGO kinetics of Inconel 718 are the aluminum diffusion in the alloy matrix and the oxygen diffusion along the interface between the alloy matrix and the oxidized grain boundary.

Keywords High-temperature oxidation · Intergranular Oxidation · Ni-based superalloy · Inconel 718

Introduction

In polycrystalline alloys, grain boundaries (GBs) can act as shortcuts for diffusion and hence can undergo preferential oxidation [1]: This phenomenon is known as intergranular oxidation (IGO). The resulting oxidized GBs can reduce the mechanical strength of the alloys by acting as both initiation sites for cracks and assist in crack propagation, resulting in premature failure [1, 2]. Therefore, in order to predict the behavior of alloys in oxidizing environments, it is important to understand the IGO mechanism and model its kinetics. Several works attempted to deal with this subject. Y. Shida et al. [1] studied the oxidation of several Ni–Al

Extended author information available on the last page of the article

Published online: 30 July 2024

binary alloys for temperatures ranging from 800 to 1100 °C and classified various types of IGO, based on different intergranular oxide morphologies. They also concluded that IGO occurs due to the diffusion of oxygen along the incoherent interface between the GB oxide and the metallic matrix. F.H. Stott et al. [3] studied the oxidation behavior of several Ni–Cr–Al ternary alloys, at 1000 °C and 1200 °C, and observed Al-rich oxide formation along the GBs. They made the hypothesis that the IGO rate-controlling step might depend not only on oxygen diffusion at the IG oxide/metal interface but also on Al diffusion inside the alloy grains when Al supply from the areas next to the grain boundaries starts to be exhausted. The same authors also put forward the role of pore formation at GBs due to vacancy condensation, which can help IGO nucleation. On the contrary, a recent work on Fe–Si and Fe–Mn model alloys [4] suggested that the kinetics of intergranular oxidation is controlled only by oxygen diffusion at the interface between oxide in GB and metallic matrix, which was found to be 60–70 times faster than the diffusion of oxygen inside the alloy grain for Fe–Si alloys.

Although there are several works which attempted to experimentally deal with IGO [1–4], very few tried to model its kinetics and today there is no recognized model for IGO. K. Jahns et al. [5] developed a numerical model for IGO using the cellular automata approach, taking into account both the oxygen diffusion in GBs and the segregation of reactive elements (like Al) along the GB.

More recently, T. Sanviemvongsak et al. proposed an analytical approach to describe the IGO kinetics [6]. Their work focused on the oxidation behavior of the Ni-based Inconel 718 alloy at 850 °C, in air. In these conditions, even if forming a Cr_2O_3 external scale, the alloy is subject to IGO: oxides rich in Al and Ti are observed in the GBs. These authors studied the maximum depth of IGO (d_{IGOmax}) as a function of time and observed a parabolic dependency, as shown by Eq. 1:

$$d_{\mathrm{IGOmax}} = \sqrt{k_{p\mathrm{IGO}} \cdot t} \tag{1}$$

where $k_{p\mathrm{IGO}}$ is the kinetic constant and t is the time.

The parabolic behavior suggests a diffusion-controlled process. Therefore, Sanviemvongsak et al. tried to apply Wagner's theory of internal oxidation to IGO. They suggested a mechanism which involves two competing processes. The first is the inward diffusion of oxygen toward the tip of the intergranular oxidation front, along the incoherent interface between the intergranular oxide and the alloy matrix; and the second is the outward diffusion of Al and Ti, first in the bulk of the grain, toward the nearest GB, and then along GBs toward the tip of the oxidation front. The authors used the Wagner equation of internal oxidation [7] for the IGO parabolic constant:

$$k_{p_{\mathrm{IGO}}} = \frac{\pi}{D_B}\left(\frac{D_O N_O}{2\gamma N_B}\right)^2 \tag{2}$$

where D_B is the bulk diffusion coefficient of the metallic species B (Al or Ti), whose oxide forms in the GB, D_O is the oxygen diffusion coefficient at the oxide/matrix interface, N_O is the oxygen concentration in the alloy, below the oxide scale and γ is

a stoichiometric coefficient. The analytical k_{pIGO} expressed by Eq. 2 was shown to be in good agreement with the experimental IGO kinetics observed in their work and previous ones when D_B was taken as the bulk diffusion coefficient of Al.

The objective of the present work is to verify the validity of the model proposed by Sanviemvongsak et al. for the IGO of Inconel 718 alloy at 850 °C, over a wider temperature range. To this aim, the intergranular oxidation behavior of this alloy was investigated for temperatures ranging from 650 up to 900 °C, in a furnace with natural convection. Oxidation experiments were performed for durations up to 5000 h and new IGO data were obtained by systematic microscopic characterizations. These data are herein compared to the model just described.

Experimental Procedures

The Inconel 718 alloy (or IN718) is a Ni-based superalloy, widely used in the aeronautical field for its good mechanical properties and high-temperature oxidation resistance. The alloy used in this study is a wrought alloy, whose nominal composition is given in Table 1. The alloy was thermally treated at 750 °C for 8 h in argon and then cooled until 620 °C at 50 °C/h, before being held again at 620 °C for 8 h and finally air-cooled. The final microstructure consists of equiaxed grains with an average grain size of 7 µm, as shown in Fig. 1. The alloy has a significant content of δ-Ni_3Nb phase, corresponding to the brighter elongated precipitates visible in Fig. 1. The measured surface fraction of the δ precipitates is around 4.5%. It is likely that the alloy also presents γ' and γ" precipitates, but the characterization of these phases is hard as they are expected to be in the submicron scale [8].

For the oxidation experiments, the alloy was cut into rectangular plates of $15 \times 10 \times 2 mm^3$; a hole 2.5 mm in diameter was drilled on each specimen in order

Table 1 Nominal composition of the IN718 alloy (wt.%)

Ni	Cr	Fe	Nb	Mo	Al	Ti
Balance	18.0	18.1	5.4	3.0	0.5	1.0

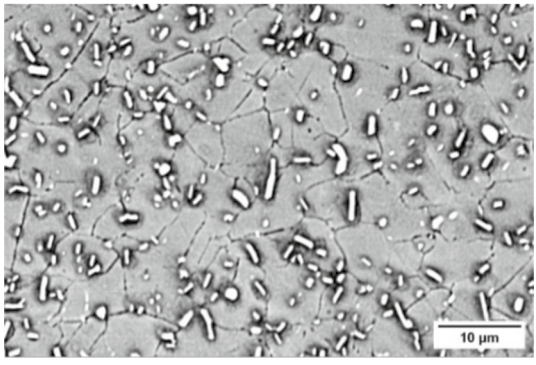

Fig. 1 Micrograph of the wrought IN718 alloy (prior to oxidation) obtained by scanning electron microscopy (SEM) in back scattered electron (BSE) mode

to hang them inside the furnace through an alumina rod. The alloy samples were ground with P600 grade with SiC paper and ultrasonically cleaned.

To statistically determine the average and maximum depth of IGO, several micrographs were analyzed. The magnification and number of micrographs were adapted to each sample in order to analyze, for all conditions, the same scan length (320 µm) below the external oxide scale. This corresponded to about 40–50 GBs observed for each sample. The quantification of intergranular oxidation was carried out using Image J software.

Results

Global Oxidation Kinetics

The mass variations per unit area $\Delta m/S$ recorded for all the oxidized IN718 samples are reported in Fig. 2 as a function of the square root of time. It can be noticed that, at each temperature, the mass variations are consistent among the various oxidized samples (up to 3), proving the repeatability of the experiments.

At 900 °C, the mass appears to continuously increase, while at 650 °C and 700 °C there is first an increase (up to 50 h), followed then by a net mass loss. This can be explained by either volatilization or spallation of the external scale. However, when the external scale was characterized using SEM, the images of the oxide scale showed no signs of spallation. Therefore, the mass loss is most likely due to volatilization. The kinetics of mass change in case of oxide growth controlled by diffusion and simultaneous oxide volatilization can be described by equation Eq. 3:

$$\frac{dm}{dt} = \frac{k'_p}{2m_o} - k'_v \tag{3}$$

where m is the net mass change of the sample per unit surface area, t is the oxidation time, m_o is the mass of oxygen in the oxide scale per unit surface area, k'_p is the parabolic constant for mass gain due to oxide scale growth and k'_v is the volatilization

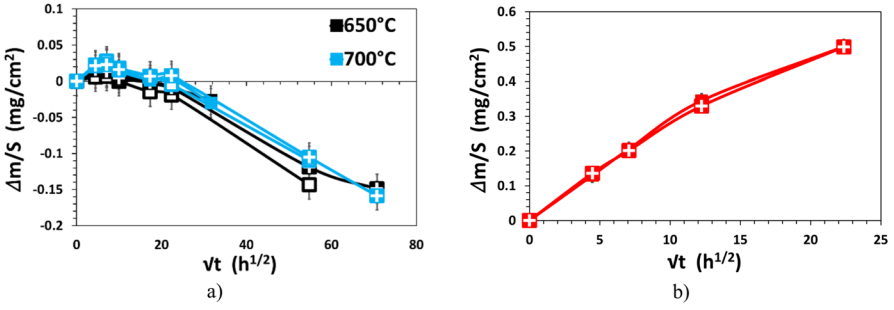

Fig. 2 Observed mass variations per unit area of the wrought IN718 alloy oxidized at 650 °C (**a**), 700 °C (**a**) and 900 °C (**b**)

rate constant of the oxide per unit surface area. The values of k'_p and k'_v were obtained by fitting the experimental mass changes according to Eq. 3, using a numerical approach. The obtained k'_p values are $6{\cdot}10^{-11}$, $3{\cdot}10^{-10}$ and $3{\cdot}10^{-7}$ $mg^2{\cdot}cm^{-4}{\cdot}s^{-1}$, respectively, for oxidation at 650 °C, 700 °C and 900 °C, with an activation energy of 314 kJ/mol. The k'_v values are $1.3{\cdot}10^{-8}$, $1.5{\cdot}10^{-8}$ and $1.5{\cdot}10^{-7}mg{\cdot}cm^{-2}{\cdot}s^{-1}$ at 650 °C, 700 °C and 900 °C, with an activation energy of 94.5 kJ/mol. The activation energy for volatilization is hence much lower than that of oxidation, which explains why the effect is more evident at low temperature. Moreover, the obtained value of 94.5 kJ/mol is close to the activation energy reported for the volatilization of $CrO_2(OH)_{2(g)}$ (112 kJ/mol) reported for Ni25Cr alloys oxidized in humid air (5 vol.% of water vapor) [9], as well as other values reported for chromia-forming alloys [10, 11]. Moreover, the curves of mass loss, shown in Fig. 2, matched well with those observed by Unocic et al. [10], for oxidation of IN718, at 650 °C and 700 °C in an air containing 10 vol.% of water vapor. It can hence be concluded that the main volatilizing species is $CrO_2(OH)_2$, whose formation is likely due to the natural humidity of the laboratory air. Indeed, humidity in the laboratory is about 2 vol.% of water vapor.

Characterization of the Oxide Scale and Grain Boundary Oxides

The X-ray Diffraction (XRD) patterns obtained at the end of oxidation for the IN718 samples oxidized at three temperatures are shown in Fig. 3. At 900 °C, several oxides are observed: Cr_2O_3 and, with less intensity, Ni–Cr spinel and TiO_2. At 650 °C and 700 °C, the most visible oxide is Cr_2O_3 and only very small traces of TiO_2 are detectable in the XRD patterns. For each sample, and in particular for those oxidized at 650 and 700 °C, the γ-phase and the δ-phase of the alloy are visible. This implies that the external scale formed on the IN718 samples is thin.

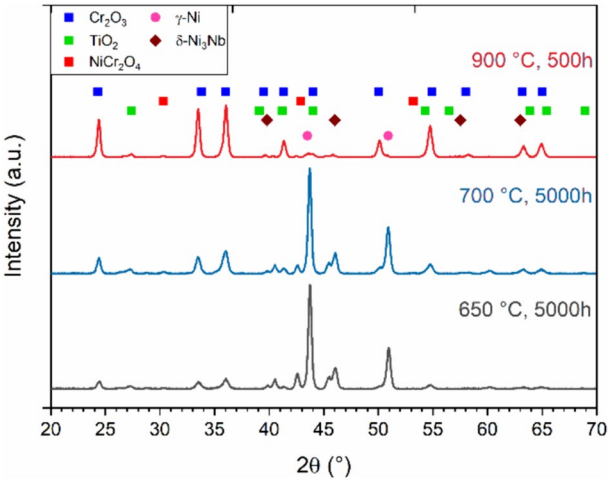

Fig. 3 XRD patterns obtained on the wrought IN718 alloy oxidized at 650 °C, 700 °C (5000 h) and 900 °C (500 h)

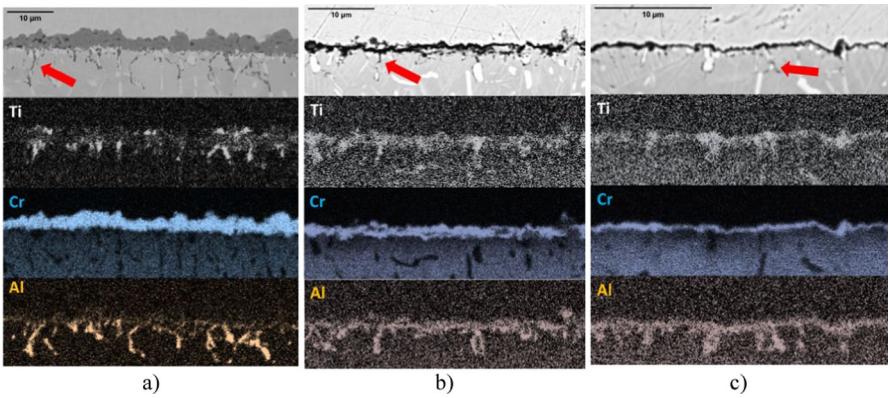

Fig. 4 SEM/BSE micrographs + EDS maps of wrought IN718 alloy oxidized **a** for 500 h at 900 °C, **b** for 5000 h at 700 °C and **c** for 5000 h at 650 °C (red arrows pointing at IGO) (Color figure online)

Table 2 Nature of oxide scales for oxidation at various temperatures obtained on the wrought IN718 alloy

Temperature (°C)	Time (h)	External scale		Intergranular oxide (IGO)		
		Main oxide	Thickness (μm)	Composition	Max depth of IGO (μm)	Average depth of IGO (μm)
650	5000	Cr_2O_3	0.28 ± 0.2	Rich in Al and Ti	3.3	2.4 ± 0.5
700	5000	Cr_2O_3	0.96 ± 0.3	Rich in Al and Ti	5.2	4.3 ± 0.5
900	500	Cr_2O_3	3.3 ± 0.2	Rich in Al and Ti	10.5	8.1 ± 1.4

The SEM/EDS analysis performed on the cross sections of the oxidized samples at the end of the oxidation is shown in Fig. 4, and the major results are summarized in Table 2. As expected from the XRD data, the SEM images confirm that the external scales are thin, being less than 1 μm for 650 and 700°C and about 3 μm for 900 °C. Oxides along the GBs are also clearly visible.

For all the three temperatures, the EDS analyses on the cross sections confirm that the oxide scale is composed mostly of chromium and oxygen, with non-homogenous titanium-rich spots. This is also consistent with XRD data. Below the oxide scale, in the metal, the oxides along the GBs are rich in Al and Ti. However, titanium is observed only up to a certain distance from the scale, while aluminum is present deeper inside the oxidized GBs. This was also previously observed by Sanviemvongsak et al., for oxidation at 850 °C up to 3000-h durations [6].

The maximum penetration depth of intergranular oxidation was obtained by image analysis of the SEM micrographs ("Materials and Methods" section), and the values are shown in Fig. 5a as a function of the square root of time. For 650 °C and 700 °C, three different durations are reported (1000, 3000 and 5000 h) and

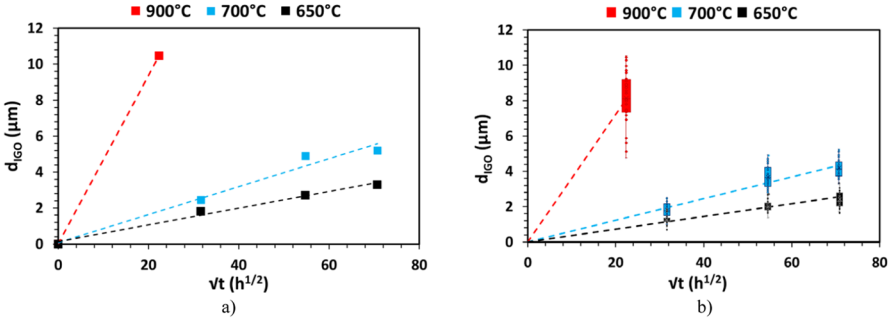

Fig. 5 **a** Evolution of the maximum penetration depth of IGO and **b** whisker plots of IGO penetrations as a function of the square root of time for the IN718 alloy oxidized in air at 650 °C, 700 °C and 900 °C

the values clearly display a linear relation on the graph. This confirms that the IGO kinetics is parabolic for the temperature/duration ranges investigated in this work. Figure 5b shows the whisker plots of all the measured penetration depths d_{IGO} obtained from image analysis, for oxidation of IN718 at 650 °C, 700 °C and 900 °C.

Discussion

For the entire temperature range of this study (650–900 °C), the external scale is composed mainly of Cr_2O_3, in agreement with the literature, reporting a chromia-forming behavior for IN718. IGO occurs at all the three studied temperatures and the oxides present at the GBs are rich in Al and Ti. Ti is present only in the oxidized GBs closer to the scale, while aluminum is also in the deepest oxides. In order to understand these differences among the observed oxide species, thermodynamic calculations were performed using the Thermo-Calc software with TCNI9 database. Figure 6 shows the mole fractions of the stable phase at 900 °C, for the IN718 composition, as a function of the oxygen partial pressure (P_{O_2}) in the system. For P_{O_2} higher than 10^{-7} atm, no metallic phases are expected to be stable and all the elements are distributed in oxides (NiO, spinel, etc.). At the beginning of the oxidation, the oxygen partial pressure at the surface of the alloy is equal to that of the atmosphere (0.21 atm for air). However, because of kinetic factors not predictable by thermodynamics, the quick formation of a Cr_2O_3 protective layer occurs. This results in a decrease of the P_{O_2}, just below the scale, to a value corresponding to the equilibrium between the alloy and the Cr_2O_3 external layer. According to the calculations shown in Fig. 6, at 900 °C, the P_{O_2} below the scale can reach a maximum of 10^{-18} atm, hence considerably lower than that of the atmosphere. Only oxide species stable for such low P_{O_2} can form in the alloy GBs. Figure 6 shows that these possible oxides are (in decreasing order of P_{O_2}) Nb, Ti and Al oxides. In particular, Al_2O_3 is the oxide observed at the lowest P_{O_2} values, in agreement with the observations of Al-rich oxides in the deepest oxidized GBs. Indeed, due to the diffusion of O in the alloy matrix, the oxygen

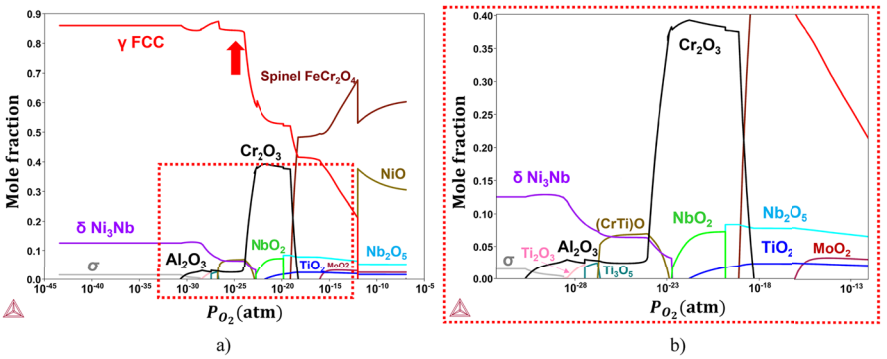

Fig. 6 **a** Evolution of stable phases of IN718 as a function of P_{O_2} at 900 °C, obtained through thermodynamic calculation. **b** Zoomed image of stable phases at low P_{O_2}

partial pressure decreases from the surface of the alloy toward its bulk. Similar results were obtained for the calculations performed at lower temperatures (not shown here).

Concerning the IGO kinetics, the results of this work have clearly confirmed a parabolic evolution of the maximum penetration depth for IN718, as previously reported at 850 °C [6]. Therefore, the slopes from Fig. 5a were used for the calculation of the IGO kinetic constant k_{pIGO}, at the three different temperatures of this study. The values are summarized in Table 3.

The k_{pIGO} herein obtained are compared to other values from the literature, over a wider temperature range, on an Arrhenius plot, shown in Fig. 7a [1, 6, 12–18]. These k_{pIGO} values are not always available in standardized form and were mostly obtained by us, by manually measuring d_{IGOmax} from published images. A general good agreement can be noticed among these data, which are well aligned, indicating that the data obey an Arrhenius-type law. This is another indication that the mechanism controlling the IGO kinetics could be controlled by diffusion. The apparent activation energy of k_{pIGO} (red line in Fig. 7a) was found to be 164 kJ/mol.

Nevertheless, it is hard to directly verify the validity of the Wagner's theory for internal oxidation adapted to IGO, as proposed by Sanviemvongsak et al. [6]. Indeed, a direct comparison between experimental k_{pIGO} and theoretical values from Eq. 2 is difficult to make because, in order to calculate theoretical k_{pIGO}, several data are needed. The bulk diffusion coefficient of aluminum D_{Al}^{bulk} is available in the literature [19]. The stoichiometric coefficient γ is 3/2 for Al_2O_3. The oxygen concentration N_O can be obtained by thermodynamic calculations, assuming that the N_O corresponds to the concentration value in the alloy depleted in all oxidized elements (Al,

Table 3 k_{pIGO} (μm²/h) of IN718 alloy

900 °C	$2.2 \cdot 10^{-1}$ [0–500 h]
700 °C	$6.3 \cdot 10^{-3}$ [0–5000 h]
650 °C	$2.4 \cdot 10^{-3}$ [0–5000 h]

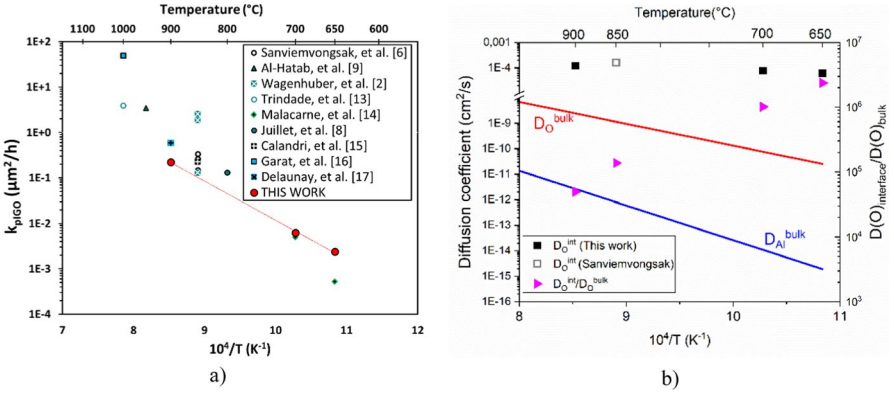

Fig. 7 **a** Arrhenius plot of k_{pIGO} for 718 alloys oxidized at different temperatures. **b** Diffusion coefficients (left axis) and ratio between interface and bulk oxygen diffusion coefficients (right axis)

Ti and partially Cr) at equilibrium with the chromia scale (Fig. 6a, red arrow). The N_O values computed using Thermo-Calc were: $1.8{\cdot}10^{-4}$ ppm at 900 °C, $1.9{\cdot}10^{-6}$ ppm at 700 °C and $1.0{\cdot}10^{-6}$ ppm at 650 °C. However, no experimental data are available for the oxygen diffusion coefficient at the Al_2O_3/alloy interface (D_O^{int}) for IN718 and the calculation of such data from fundamental numerical approaches is out of the scope of this work. The calculation was hence reversed in order to obtain D_O^{int} from the experimental k_{pIGO}, assuming the model to be correct. The obtained values are shown and compared to the bulk diffusion coefficient of oxygen in nickel D_O^{bulk} [20] in Fig. 7b. The obtained D_O^{int} values only slightly increase with temperature in the studied range, while the D_O^{int}/D_O^{bulk} ratio decreases. Moreover, it can be noticed the obtained D_O^{int} values (black squares) fall well on a line in the Arrhenius plot reported in Fig. 7b, and hence, they can be fitted according to an Arrhenius law:

$$D_O^{int} = D_o e^{\frac{-Q}{RT}} \tag{4}$$

where D_o is the pre-exponential factor, equal to $3.1{\cdot}10^{-3}$ cm^2/s, Q is the activation energy, found to be 30 kJ/mol (calculated from data, Fig. 7b)), R is the gas constant and T is the temperature. This is consistent with diffusion theory, because the activation energy for interfacial diffusion is much lower than that found for diffusion in the bulk (164 kJ/mol), as expected. Moreover, D_O^{int}/D_O^{bulk} ratios are in the order of 10^5–10^6, which is consistent with previous data obtained on model Ni–Al alloys by Stott et al. [21].

Equation 2 can be re-arranged to show that the activation energy of k_{pIGO} is related to the activation energies of N_O, D_O^{int} and D_{Al}^{bulk}, according to Eq. 5:

$$Q_{k_{pIGO}} = 2\left(Q_{N_O} + Q_{D_O^{int}}\right) - Q_{D_{Al}^{bulk}} \tag{5}$$

In the present study, the variables k_{pIGO}, D_O^{int}, D_B and N_O all follow an Arrhenius behavior with activation energies found to be 164 kJ/mol, 30 kJ/mol and 260 kJ/

mol [19], respectively. The variation of N_O with temperature is less obvious, but it was found to be also an Arrhenius-type law. This result, obtained by thermodynamic calculations, could be inferred by the Sievert's law and Van't Hoff equation in Eq. 6:

$$N_O \propto K\sqrt{\frac{P_{O_2}}{P_o}}e^{\left[-\frac{H^S}{RT}\right]} \tag{6}$$

where P_{O_2}, is the partial pressure of oxygen, P_o is 1 atm and H^S is the activation energy for dissolution. In the original formulation of Sievert law, P_{O_2} is the partial pressure of oxygen in the gas at the equilibrium with the metal. In this case, this is the oxygen partial pressure imposed by the oxide (Cr_2O_3)/metal equilibrium. This P_{O_2} follows a "perfect" Arrhenius law only for pure metals. For alloys, a correction for the chemical activity of the metallic species (a_{Cr}) has to be added, as shown in [22]. However, it was found out that the P_{O_2} variation, in the range 650–900°C, follows also an Arrhenius law, indicating that the variation of chromium activity is limited. Therefore, N_O follows an Arrhenius law, with an activation energy found to be 189 kJ/mol from our thermodynamic calculations.

Conclusions and Perspectives

New data on the intergranular oxidation behavior of grade Inconel 718 alloy, for temperatures ranging from 650 to 900 °C, were provided in this work. A systematic statistical analysis has shown that both the average and the maximum penetration depth of IGO evolve with time according to a parabolic law. The corresponding $k_{p\mathrm{IGO}}$ parabolic constants obtained from our experimental data, as well as those obtained from the literature review, vary as a function of temperature according to an Arrhenius law, with an apparent activation energy of 164 kJ/mol. These results confirm the model recently proposed by Sanviemvongsak et al. [6]. In this model, Wagner's theory of internal oxidation is extended to IGO with two competing processes: the diffusion of oxygen at metal/intergranular oxide interface and the bulk diffusion of aluminum. This work also points out the need for diffusion coefficient data that are rare in the literature, especially concerning oxygen diffusion along grain boundaries and oxide/alloy interfaces. Indeed, this will be essential to have quantitative and reliable models to predict intergranular oxidation.

Acknowledgements This work was performed in the frame of the research project COMEHT (Corrosion, Oxidation, Mechanics, High Temperature), managed by Institut de Recherche Technologique: Matériaux Métallurgie Procédés (IRT M2P). The authors acknowledge IRT M2P, their industrial partners (Safran Group, CEA, Aperam, Veolia, Saint-Gobain) and academic partners (CIRIMAT, UTC, IJL, EMSE).

Author Contributions S. M. performed experimental work and modeling and wrote the main text. E. E. worked on the thermodynamic modeling, supervised the work and participated in the writing of the main text. T. S. supervised the work, advised on experimental analysis and provided the materials. D. Ma. provided the funding and supervised the experimental work. J. F. and D. Mo. directed and supervised the entire work. D. Mo. participated in the analysis of the experimental data too. All authors reviewed the manuscript.

Funding Open access funding provided by Institut National Polytechnique de Toulouse. This work was financially supported by the French program Plan d'Investissement d'Avenir (PIA).

Data Availability No datasets were generated or analyzed during the current study.

Declarations

Conflict of interest The authors declare no competing interests.

References

1. Y. Shida, F. H. Stott, B. D. Bastow, et al., *Oxidation of Metals* **18**, 1982 (93–113).
2. Wagenhuber, E. G., VBd Trindade, and U. Krupp, *In Proceedings International Symposium Superalloys Var. Deriv*, (Pittsburgh, PA., 2005).
3. F. H. Stott, G. C. Wood, Y. Shida, et al., *Corrosion Science* **21**, (8), 1981 (599–624).
4. Ronqueti, L. A., Favergeon, J., Risbet, M., et al., *53th Seminario de Laminacao* 283–292 (2016).
5. K. Jahns, K. Balinski, M. Landwehr, et al., *Oxidation Metals* **87**, 2017 (285–295).
6. Sanviemvongsak, T., Monceau, D., Desgranges, C., et al., *Corrosion Science*, 170, 108684 (2020).
7. D. J. Young, *High Temperature Oxidation and Corrosion of Metals* (Elsevier Science, Amsterdam, 2008).
8. Azadian, S., Wei, L. Y., and Richard Warren, *Materials Characterization*, 53, 1, 7–16 (2004).
9. G. R. Holcomb and D. E. Alman, *Scripta materialia* **54**, (10), 2006 (1821–1825).
10. Unocic, K. A., Unocic, R. R., Pint, B. A., et al. *In Proceedings of the 7th International Symposium on Superalloy*, 718 (2010).
11. P. Berthod, *Oxidation of Metals* **64**, (3), 2005 (235–252).
12. C. Juillet, A. Oudriss, J. Balmain, et al., *Corrosion Science* **142**, 2018 (266–276).
13. Kh. A. Al-Hatab, M. A. Al-Bukhaiti, U. Krupp, et al., *Oxidation Metals* **75**, (3), 2011 (209–228).
14. R. Malacarne, S. Mathieu, L. Aranda, et al., *Corrosion Science* **188**, 2021 109500.
15. M. Calandri, D. Manfredi, F. Calignano, et al., *Advanced Engineering Materials* **20**, (11), 2018 (1800351).
16. Garat, V., Deleume, J., Cloué, J. M., et al., *In: Superalloys* 718, 625 559–569 (2005).
17. F. Delaunay, C. Berthier, M. Lenglet, et al., *Microchimica Acta* **132**, (2), 2000 (337–343).
18. V. B. Trindade, U. Krupp, P. E. G. Wagenhuber, et al., *Materials at High Temperature* **22**, (3–4), 2005 (207–212).
19. W. Gust, M. B. Hintz, A. Loddwg, et al., *Physica Status Solidi (a)* **64**, (1), 1981 (187–194).
20. J. W. Park and C. J. Altstetter, *Metallurgy Transactions A* **18**, (1), 1987 (43–50).
21. F. H. Stott and G. C. Wood, *Materials Science and Technology* **4**, (12), 1988 (1072–1078).
22. E. Epifano and D. Monceau, *Corrosion Science* **217**, 2023 111113.

Authors and Affiliations

Sudhanva Madhusudan[1,3] · Enrica Epifano[1] · Jérôme Favergeon[2] · Tom Sanviemvongsak[4] · David Maréchal[3] · Daniel Monceau[1]

✉ Enrica Epifano
enrica.epifano@toulouse-inp.fr

Sudhanva Madhusudan
sudhanva.madhusudan@toulouse-inp.fr

Jérôme Favergeon
jerome.favergeon@utc.fr

Tom Sanviemvongsak
tom.sanviemvongsak@safrangroup.com

David Maréchal
david.marechal@irt-m2p.fr

Daniel Monceau
daniel.monceau@toulouse-inp.fr

[1] CIRIMAT Laboratory, University of Toulouse, CNRS, INPT, UPS, ENSIACET, 4 allée Emile Monso, BP-44362, 31030 Toulouse Cedex 4, France

[2] Laboratoire Roberval, Université de Technologie de Compiègne, Compiègne, France

[3] Institut de Recherche Technologique - Matériaux Métallurgie et Procédés, Metz, France

[4] Safran Tech, Rue des Jeunes Bois, Châteaufort, CS 80112, 78772 Magny-Les-Hameaux, France